

32.0 DEVELOPMENT OF CABINET BASED COMPUTED TOMOGRAPHY METHODS FOR STUDIES OF MICROSTRUCTURES AND DEFECTS IN METALS (LEVERAGED)

C. Gus Becker (Mines)

Faculty: Amy Clarke (Mines)

Industrial Mentor: Michelle Espy (LANL)

This project initiated in Fall 2017 and is supported directly by Los Alamos National Laboratory (LANL). The research performed during this project will serve as the basis for a Ph.D. thesis program for C. Gus Becker.

32.1 Project Overview and Industrial Relevance

X-ray radiography allows for the imaging of materials in a non-destructive manner by observing X-rays transmitted through the material. This method can be used for post-mortem analysis, as well as in-situ imaging of microstructural development. For example, dynamic imaging of microstructural evolution during processing (e.g. casting or directional solidification) can further our understanding of the mechanisms driving microstructural development, improving predictive capabilities [32.1]. X-ray radiography can also be used to capture multiple images of a sample from different angles, which can be reconstructed and represented as a three-dimensional model. A reconstruction of a metal sample created through additive manufacturing (AM) can be generated to reveal microstructural characteristics and internal defects. Reconstructions can also be created from four-dimensional microscopy (three spatial and one temporal dimension), in which images are collected from different angles of a time-evolving sample. These reconstructions are created using techniques like the Time-Interlaced Model-Based Iterative Reconstruction (TIMBIR) [32.2], which improves temporal resolution to capture microstructural evolution during processing.

Synchrotron X-ray sources can be used to obtain high-spatial resolution X-ray radiographs (on the order of 1 μm), however these images have a small field of view and require significant beam time at a national user facility. High-energy micro-focus X-ray radiography has the drawback of lower spatial resolutions, but increases the field of view significantly and can be performed in a laboratory. These laboratory instruments consist of a high-energy micro-focus X-ray source, radiation shielding (typically in the form of a lead-lined cabinet housing the source), a scintillator to convert X-rays to visible light, and a camera/detector to collect that light. Tomographic data can be obtained when a rotation stage is included to rotate the sample. Solidification experiments are often performed at synchrotron X-ray facilities like the Advanced Photon Source (APS) at Argonne National Laboratory (ANL), as well as in facilities with micro-focus X-ray capabilities like the non-destructive testing group (E-6, formerly AET-6) at Los Alamos National Laboratory (LANL) to study the microstructures and properties of materials. Many experiments have been performed by CANFSA faculty and students at Mines to study different aspects of alloy solidification, such as crystal growth and solute segregation [32.1], primary dendrite spacing and size [32.3], dendrite fragmentation [32.4], and the effect of different cooling rates on solidification [32.5].

When X-ray radiography and computed tomography are used for the non-destructive imaging of metals, sample thickness is a constraint for high density alloys. X-rays at national user facilities (with energies of ~ 30 keV) can typically penetrate thin foils of material (~ 100 μm to ~ 1 mm) to image thin sections or small volumes to produce computed tomographic reconstructions [32.5], but typically cannot be used to image thicker or larger samples, unless special high-energy beamlines are used with X-ray energies up to ~ 150 keV. High-energy micro-focus X-ray imaging utilizes X-rays with energies of up to 250 keV and beyond, allowing sample thicknesses on the order of millimeters, and larger fields-of-view on the order of centimeters. Proton radiography (pRad), in which 800 MeV energy protons are transmitted through samples at LANL's Los Alamos Neutron Science Center (LANSCE), allows for even larger sample sizes and the ability to probe materials with high atomic numbers, albeit at the cost of lower spatial resolution [32.1]. There have also been proof-of-concept experiments of Transmission High-Energy Electron Microscopy (THEEM), in which extremely high-energy electrons (15 GeV) are transmitted through samples at the Stanford Linear Accelerator Center (SLAC) to achieve deeply penetrating electron radiography [32.6]. This method has yet to be optimized, but holds potential for high atomic number (Z) materials. The goal of this project is to establish high-energy (~ 160 keV), micro-focus X-ray imaging in the laboratory at Mines with capabilities between those of synchrotron facilities and pRad (*i.e.* ~ 5 μm spatial resolution and $\sim 2 \times 3$ cm fields-of-view).

32.2 Previous Work

Prior to the start of this project, *in-situ* solidification was studied using synchrotron X-ray imaging at the APS and using high-energy micro-focus X-ray radiography systems in a laboratory setting on site at LANL, in collaboration with E-6. An image processing method has been created to process the data from these experiments. Once processed, this data can be analyzed to capture phenomena like the multiscale solidification dynamics in metallic alloys, or simulated AM and related defects, for example. This image processing method, developed at the beginning of this project, consists of modular ImageJ macros that each take a directory of images from an experiment and performs a programmed process to enhance the images in some way, saving the results as separate files to preserve the original, unedited images. The modular nature of these scripts allows for processing steps to be reperformed in different sequences on the original images, adding to or changing the image processing steps to achieve different results and quantitatively describe dynamic events.

This image processing method is exhibited by processing a high-energy micro-focus solidification experiment performed with E-6 using the same experimental set-up as previous synchrotron X-ray experiments. This set-up consists of a steel bar with an rectangular window extracted to aid in the transmittance of X-rays, as seen in the directional solidification of an Al-Ag alloy in **Figure 32.1a**. Micro-focus X-ray radiography allows for a larger field-of-view than synchrotron X-ray radiography, so the experiment designed for synchrotron radiography takes place in only a fraction of the entire image captured with the micro-focus system. The first script extracts the lighter portion of the radiographs where the experiment is taking place (**Figure 32.1b**). Another script removes a set amount of pixels from each side of the images, allowing for better contrast (**Figure 32.2a**). Vertical and horizontal banding artifacts from the imaging process can be reduced with a script that performs fast Fourier transform filtering (**Figure 32.2b**).

Image processing can also be performed through programming in the Python language with the package *scikit-image* [32.7]. Some of these advanced image processing techniques have been explored with data of various compositions of solidifying Al-Ge alloys, collected by Mines CANFSA faculty and students with the Dynamic Transmission Electron Microscopy (DTEM) at Lawrence Livermore National Laboratory (LLNL). An example DTEM image is shown in **Figure 32.3a**. This data was chosen as a candidate for the exploration of Python for many reasons: the resemblance in the DTEM images to high-energy micro-focus X-ray radiographs, the high amount of noise in the data that allow for the deployment of restoration and denoising algorithms, and the juxtaposition of multiple frames in each DTEM image requiring an elaborate segmentation technique to separate the individual frames. A total variation minimization algorithm [32.8] is used to reduce noise in the DTEM data (**Figure 32.3b**). The image is then segmented, allowing each frame to be extracted from the original image, using a technique known as watershed segmentation from the *scikit-image* package (**Figure 32.4**), at which point the segmented frames can be independently extracted from the image and stitched together as an animation (**Figure 32.5**).

32.3 Recent Progress

An important image processing skill, which will become useful when Mines obtains the laboratory X-ray cabinet, is the ability to extract quantitative information from images. This can be applied to AM simulator experiments performed at the APS at ANL to extract necessary information like solid-liquid interface velocities to further understand rapid solidification. These experiments consist of a metallic sample placed in an argon back-filled chamber at an X-ray imaging beamline (Sector 32-ID) at the synchrotron. A portion of the surface of the sample is then subject to laser melting and begins to solidify. By capturing *in-situ* radiographs of this process, the position of the solid-liquid interface can be tracked over time. These measurements have been performed rather painstakingly by creating an ImageJ macro that prompts the user to manually locate the interface across many images. As a way to further develop image processing skills, Python image processing has been deployed to locate the interface automatically. The successful application of this approach results in reduced time and labor spent locating the interface in each image manually, an increase in reproducibility due to a reduction of human error in measurements, and a greater understanding of the concepts of image processing and programming with Python to be applied to other problems.

At this point, a program has been developed that can locate the solid-liquid interface across many radiographs of an AM simulator experiment of a nickel alloy, in which the interface is relatively pronounced (**Figure 32.6a – c**). This is achieved by performing an image processing routine to each image in the experiment dataset. First a Gaussian filter

is applied to smooth out noise. The preceeding image is then subtracted to highlight the differences in a new image. This corresponds to the area where the solid-liquid interface has contracted, as compared to the preceeding image, and is therefore a representation of the location of the interface at that point in time. Pixels of outlying intensity are then removed from the difference image to give better contrast. Finally, a denoising algorithm is performed. The result of this process is seen in **Figure 32.6d – f**. The next step in the process is to identify the boundaries of the interface. This can be done in Python by converting the resulting image from the processing routine to a binary image, represented of only intensities of one or zero. This is done by thresholding the processed image and setting all intensities above a certain value to one, and all intensities below that value to zero. This, combined with an algorithm that excludes regions of smaller area, results in the binary images seen in **Figure 32.7a – c**. The boundaries from these images can be overlaid on the original images to show the correlation to the unprocessed solid-liquid interfaces (**Figure 32.7d – f**). The lower boundary tracks the bottom of the solid-liquid and can be plotted with the time elapsed from the start (due to constant framerate) to reveal the nature of the movement of the interface (**Figure 32.8**).

32.4 Plans for Next Reporting Period

In the short term, the following tasks will be completed:

- Apply edge detection techniques to improve solid-liquid interface tracking in AM simulator experiments.
- Explore the *OpenCV* package in Python to further explore computer vision capabilities and create custom interactive image processing interfaces.
- Develop a methodology to create 3D models (see **Figure 32.9**) for Al alloy tomography data obtained by Brian Milligan and other CANFSA students at the APS to prepare for future tomography experiments.
- Finalize delivery of X-ray cabinet to Mines (may be delayed due to current global COVID-19 circumstances).
- Begin initial 3D tomography on AM-built lattice structure samples recently received from LANL and Sandia National Laboratories.

32.5 References

- [32.1] P.J. Gibbs, S.D. Imhoff, C.L. Morris, F.E. Merrill, C.H. Wilde, P. Nedrow, F.G. Mariam, K. Fezzaa, W.-K. Lee, A.J. Clarke, Multiscale X-ray and proton imaging of bismuth-tin solidification, *JOM*. 66 (2014) 1485–1492.
- [32.2] K. Aditya Mohan, S.V. Venkatakrishnan, J.W. Gibbs, E.B. Gulsoy, X. Xiao, M. De Graef, P.W. Voorhees, C.A. Bouman, TIMBIR: a method for time-space reconstruction from interlaced views, *IEEE Transactions on Computational Imaging*. 1 (2015) 96-111.
- [32.3] A.J. Clarke, D. Tournet, Y. Song, S.D. Imhoff, P.J. Gibbs, J.W. Gibbs, K. Fezzaa, A. Karma, Microstructure selection in thin-sample directional solidification of an Al-Cu alloy: in situ X-ray imaging and phase-field simulations, *Acta Materialia*. 129 (2017) 203-216.
- [32.4] J.W. Gibbs, D. Tournet, P.J. Gibbs, S.D. Imhoff, M.J. Gibbs, B.A. Walker, K. Fezzaa, A.J. Clarke, In situ X-ray observations of dendritic fragmentation during directional solidification of a Sn-Bi alloy, *JOM*. 68 (2016) 170-177.
- [32.5] B.M. Patterson, K.C. Henderson, P.J. Gibbs, S.D. Imhoff, A.J. Clarke, Laboratory micro- and nanoscale X-ray tomographic investigation of Al-7 at.%Cu solidification structures, *Materials Characterization*. 95 (2014) 18-26.
- [32.6] F.E. Merrill, J. Goett, J.W. Gibbs, S.D. Imhoff, F.G. Mariam, C.L. Morris, L.P. Neukirch, J. Perry, D. Poulson, R. Simpson, P.L. Volegov, P.L. Walstrom, C.H. Wilde, C. Hast, K. Jobe, T. Smith, U. Wienands, A.J. Clarke, D. Tournet, Demonstration of transmission high energy electron microscopy, *Applied Physics Letters*. 112 (2018) 144103.
- [32.7] A. Chambolle, An Algorithm for Total Variation Minimization and Applications, *Journal of Mathematical Imaging and Vision*. 20 (2004) 89–97.
- [32.8] S. van der Walt, J. L. Schönberger, J. Nunez-Iglesias, F. Boulogne, J. D. Warner, N. Yager, E. Gouillart, T. Yu, Scikit-Image: Image Processing in Python, *PeerJ*. 2 (2014) 453-471.

32.6 Figure and Tables

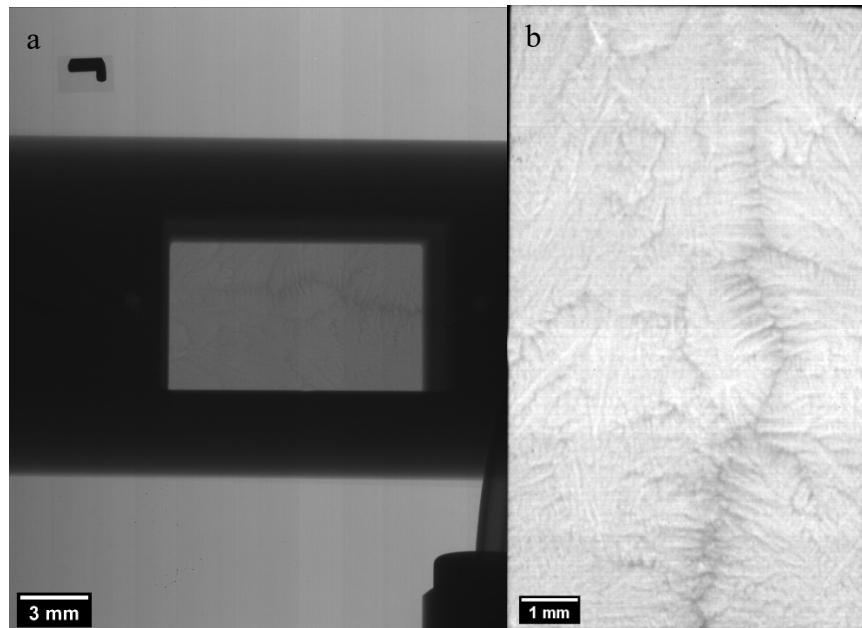


Figure 32.1: A frame from the solidification process of an Al-Ag alloy obtained using high-energy micro-focus X-ray radiography of a sample undergoing directional solidification. The experiment was performed using the synchrotron X-ray radiography experimental set-up, so the experiment is entirely contained in the small, light gray window in the center of (a) and cropped to that window and rotated in (b). The horizontal feature in (a) is a steel bar. Laboratory X-ray imaging affords new opportunities to study larger fields-of-view.

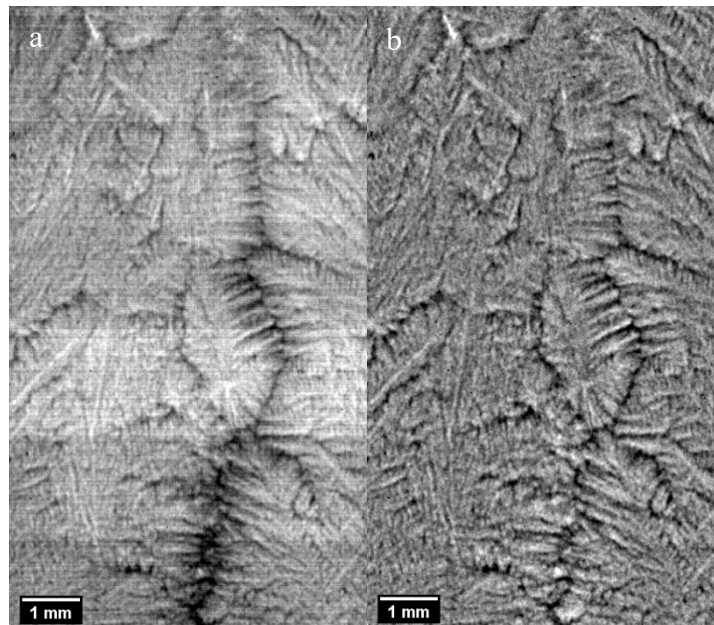


Figure 32.2: Further processing of the same frame of Al-Ag solidification shown in **Figure 32.1** by (a) trimming 10 pixels from each edge of the radiograph, allowing for better contrast in the solidification structure, and (b) performing fast Fourier transform filtering to remove horizontal and vertical banding artifacts. Note: rotated 90 degrees for presentability; gravity is to the right of the page.

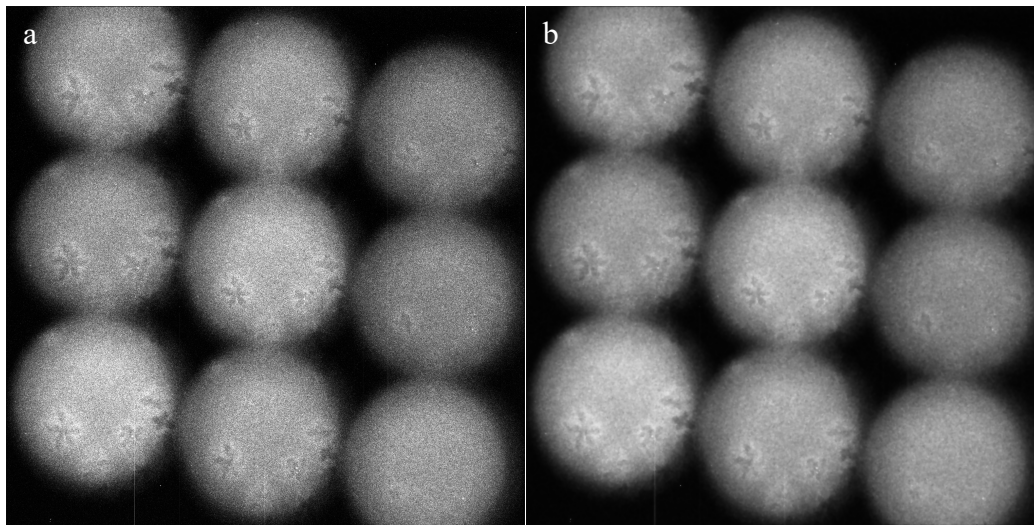


Figure 32.3: Solidification of Al-45%Ge, represented by (a) the original LLNL DTEM image, and (b) the image with applied noise reduction filter [32.7]. Each image contains nine frames, the chronological order of which begins in the lower right corner, up to the top right, left to top center, down to bottom center, left to bottom left, and up to top left.

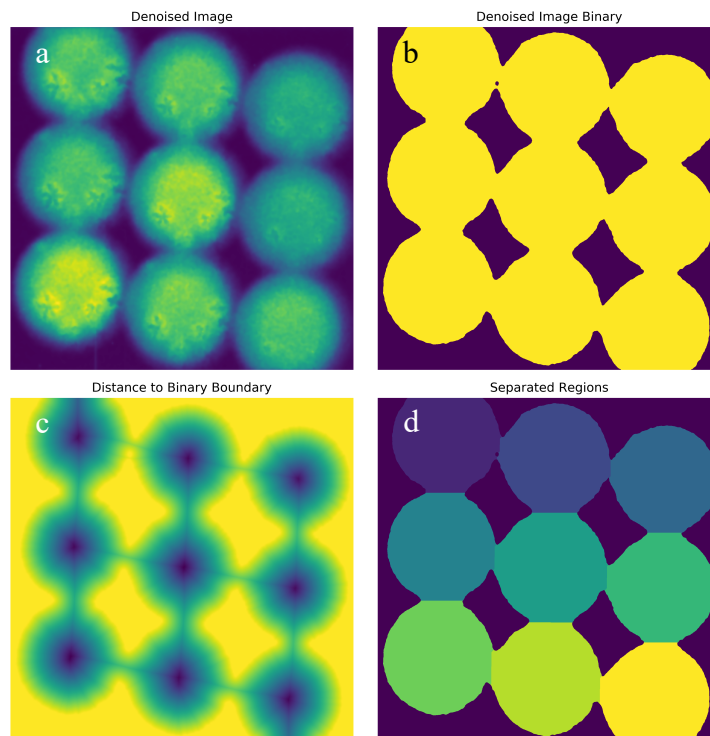


Figure 32.4: (a) Denoised Al-45%Ge LLNL DTEM image. (b) Binary mask created using the minimum thresholding method in *scikit-image*. (c) Distance map created by mapping each pixel with a value that correlates the distance to the edge of the mask. (d) Regions obtained by performing a watershed segmentation of the distance map. A purple to yellow colormap is used to more easily distinguish between pixel values.

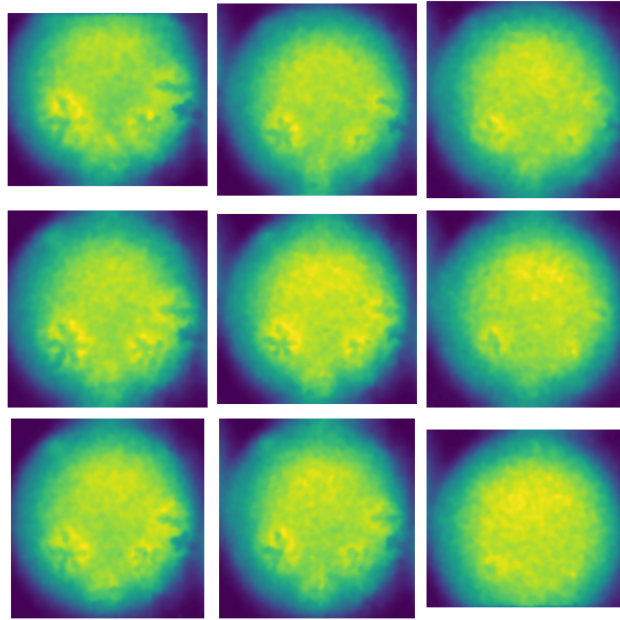


Figure 32.5: Segmented regions of the denoised Al-45%Ge DTEM image obtained by performing the watershed segmentation process, as illustrated in **Figure 32.4**.

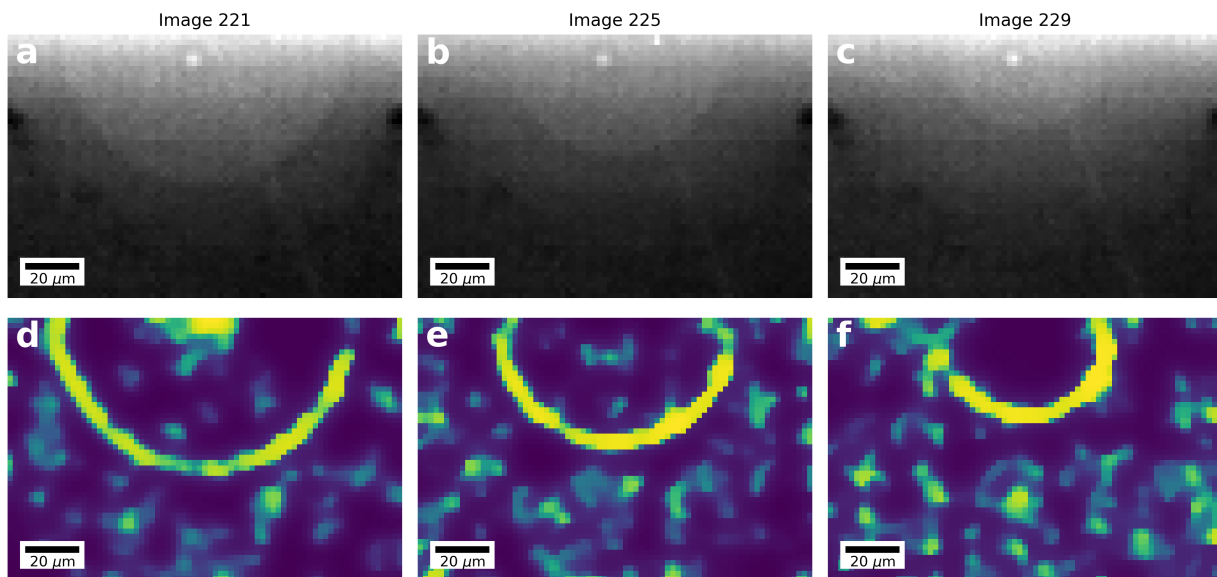


Figure 32.6: (a – c) In-situ radiography of a Ni alloy during simulated AM at the Sector 32-ID-B at the Advanced Photon Source at Argonne National Laboratory. The radiographs show three stages of solidification of a melt pool formed after laser melting. (d – f) Image processing of corresponding radiographs to detect the solid-liquid interface during solidification. This was achieved through a combination of Gaussian smoothing, subtraction of the previous image, removal of outlying pixels, and application of a denoising algorithm.

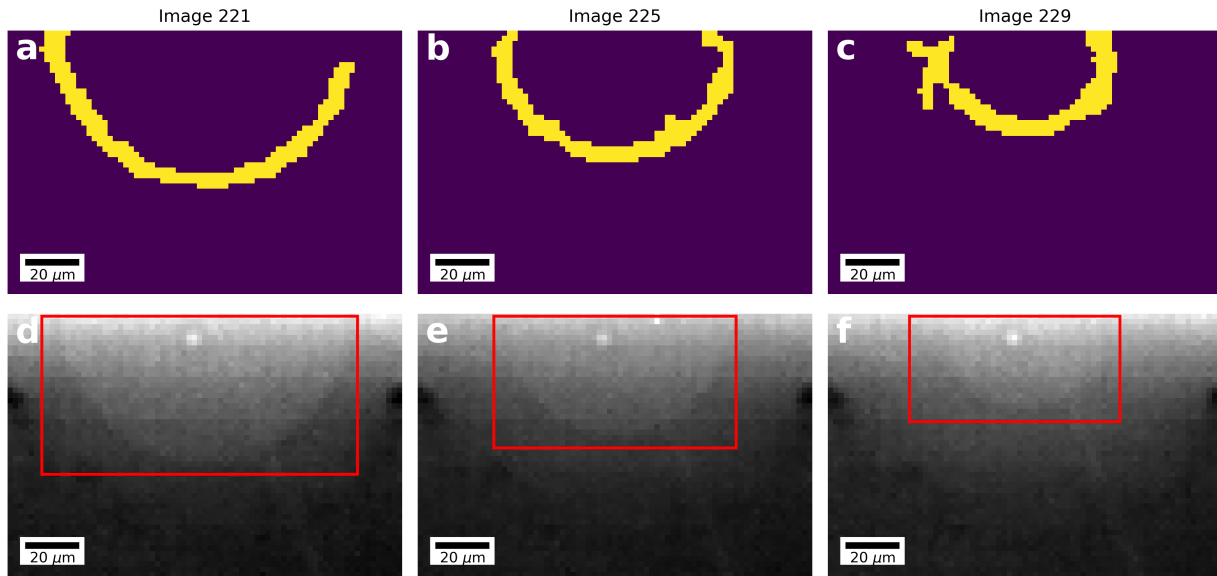


Figure 32.7: After performing the image processing displayed in **Figure 32.7d – f**, a binary image is created by thresholding all pixels above a certain intensity. (a – c) The binary images are used to track the position of the solid-liquid interface during solidification. (d – f) The boundaries of the binary images are overlaid on the unprocessed images to show the correlation.

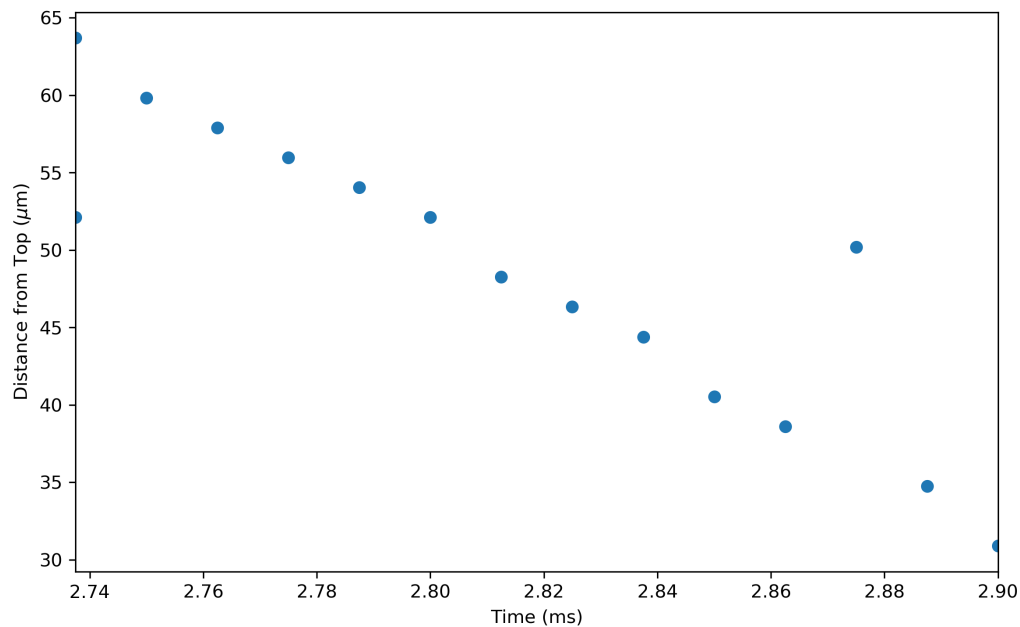


Figure 32.8: Plot of the distance of the bottom of the melt pool to the top of the image as it changes over time following the laser melting. This data was collected from the lower boundary seen in **Figure 32.7d – f**.

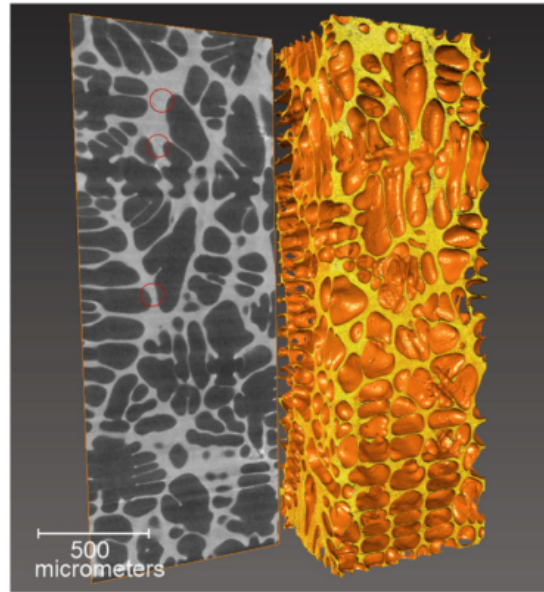


Figure 32.9: Three-dimensional tomographic reconstruction of an Al-Cu alloy from multiple radiographs. Reconstructions allow for manipulation of data unavailable from radiographs alone. The Al-rich primary dendrites in the reconstruction have been rendered translucent to better show the Cu-containing eutectic in orange [32.5].